On the Texture Formation of Selective Laser Melted Ti-6Al-4V

MARCO SIMONELLI, YAU YAU TSE, and CHRIS TUCK

Selective laser melting (SLM) has been shown to be an attractive manufacturing route for the production of α/β titanium alloys. The relationship between the SLM process parameters and the microstructure of titanium alloys has been the object of several works, but the texture formation during the SLM process has yet to be understood. In the present study, the texture formation of Ti-6Al-4V components was investigated in order to clarify which microstructural features can be tailored during the SLM process. The microstructural characterization of the as-built components was carried out using various microscopy techniques. Phase and texture analysis were carried out using backscattered electron imaging and diffraction. It was found that as-built components consist exclusively of α' martensitic phase precipitated from prior β columnar grains. The texture of the prior β phase was reconstructed and discussed in relation to the used SLM process parameters. It was found that the β grain solidification is influenced by the laser scan strategy and that the β phase has a strong $\langle 100 \rangle$ texture along its grain growth direction. The α' martensitic laths that originate from the parent β grains precipitate according to the Burgers orientation relationship. It was observed that α' laths clusters from the same β grain have a specific misorientation that minimizes the local shape strain. Texture inheritance across successive deposited layers was also observed and discussed in relation to various variant selection mechanisms.

DOI: 10.1007/s11661-014-2218-0

I. INTRODUCTION

SELECTIVE laser melting (SLM) is an additive manufacturing (AM) technique based on an infra-red fiber laser that creates solid layers from loose powder material and joins them in an additive manner. In principle, a thin layer of loose powder is initially leveled across a process platform to form a powder bed. Selected areas of the powder bed are then melted and consolidated line by line by a scanning laser. As soon as this layer is formed, new loose powder is deposited and melted on top of the layer below. Repeating this basic principle for multiple additive layers, any 3D component can then be created. SLM not only reduces waste material but also saves energy when compared to traditional processing techniques.[1,2] As the energy delivered by the laser is controllable, SLM has shown the possibility to fabricate near fully dense objects made of a wide range of metals generating interest in the aerospace and biomedical devices applications.[3,4]

Nevertheless the microstructure of α/β titanium alloys produced by SLM (*e.g.*, prior β grain morphology) differs significantly from the microstructure of the cast or wrought alloys of the same composition. The specific microstructure of the as-built SLM components is responsible for the manifested mechanical anisotropy and low ductility.[5–7] Microstructural studies of the as-built components have revealed for example large elongated prior β grains formed along the build direction filled with acicular α' martensitic laths.[8–12] It is suggested that when the laser hits the powder bed, the grains in the previous deposited layers and the powder particles of the top layer transform into the β phase field. The β grains then solidify and grow epitaxially along the direction of heat conduction (typically in a columnar way in the build direction). Finally, as the laser moves away across the powder bed multiple α' martensitic laths precipitate within the elongated columnar grain of the parent β grain. The origin of similar columnar microstructures has also been discussed in α/β titanium alloys produced by other AM systems.[13–16]

Although a number of process parameters such as laser scan speed, hatch spacing, and scan strategy have shown to play an important role in the densification mechanism of the SLM parts,[9,10,17,18] less effort has been spent to understand how these process parameters affect the solidification of the β grains, the $\beta \rightarrow \alpha'$ transformation and the texture evolution that takes place at each layer deposition. Therefore the microstructure of the α/β titanium alloys processed by SLM is not yet tailorable and specific post-treatments are required to achieve desired microstructural features.[6,7] The β grains size, boundaries, and crystallographic texture have indeed a great influence on the α phase precipitation and orientation distribution, and hence the static and dynamic mechanical properties of α/β Ti alloys.[19,20] The investigation of the α/β relationship is however complicated because generally only limited or no β phase is present at room temperature after rapid

MARCO SIMONELLI, Ph.D Researcher, and YAU YAU TSE, Lecturer, are with the Department of Materials, Loughborough University, Loughborough LE11 3TU, U.K. Contact e-mail: M.Simonelli@lboro.ac.uk CHRIS TUCK, Associate Professor, is with the Additive Manufacturing and 3D Printing Research Group, Faculty of Engineering, The University of Nottingham, Nottingham NG7 2RD, U.K.

Manuscript submitted October 3, 2013.
Article published online February 13, 2014

cooling from the β phase field. To solve this problem, several studies have shown that the β phase crystallographic texture can be reconstructed from the α phase texture *via* the Burgers orientation relationship for which the $(0001)_\alpha//(110)_\beta$ and $\langle 11\bar{2}0\rangle_\alpha//\langle 111\rangle\beta$.[21–24] A recent study conducted on the origin of texture of electron beam melted (EBM) Ti-6Al-4V has shown that the columnar β grain possess a dominant $\langle 100\rangle$ fiber texture in the grain growth direction.[15] The orientation relationship between the α phase and the parent β phase has however not been investigated in detail and no apparent variant selection is reported. To the author's knowledge, there is no study in the literature about texture formation of Ti-6Al-4V during SLM.

The present work uses orientation imaging microscopy (OIM) to study as-built SLM Ti-6Al-4V components in order to clarify whether and which microstructural features could be tailored during SLM. This work will focus on the crystallographic texture evolution of SLM Ti-6Al-4V in relation to a set of process parameters that have led to a production of near fully dense components (99.7 ± 0.2 pct dense). The $\beta \rightarrow \alpha'$ phase transformation that occurs during the deposition of each layer will also be discussed.

II. MATERIALS AND EXPERIMENTAL PROCEDURE

The SLM specimens studied in this work were built using pre-alloyed plasma atomized Ti-6Al-4V grade 23 powder supplied by LPW, UK. The powder size and distribution were initially determined using a particle size analyzer Malvern MasterSizer 2000. The powder has a measured particle size ranging from 15 to 70 μm with about 75 pct of the examined particle size that falls between 25 and 50 μm. Particles appear spherical, smooth with a few smaller condensed particles agglomerated with larger particles.[25] The microstructure of the starting powders was studied by serial cross-sectioning using a focused ion beam.[25] Its microstructure consists of lamellar α' phase with only a limited amount of retained β phase.[25] The initial powder appeared fully dense. Cubic components of 1 cm^3 were built using a Renishaw SLM250 machine.[26] The SLM250 is equipped with an infra-red fiber modulated pulse laser with a wavelength of 1070 nm and a nominal maximum power of 200 W. In this study, the maximum laser power at the workpiece was 157 W due to losses in the optical train. A series of experiments were performed to establish a processing window that could minimize residual porosity and the optimal processing parameters were reported in detail elsewhere.[27]

All the parts were built using a meander scan strategy (Figure 1). Each cross section was initially offset 100 μm from the edge. The area enclosed by the offset was scanned using alternating parallel scan vectors. The laser then scanned twice the offset boarder in order to improve the surface roughness of the parts and reduce the number of defects near the external surface of the components. It is noteworthy that the alternating parallel scan vectors were rotated by 67 deg at each new layer deposition as depicted in Figure 1. The cubes were built directly on top of a

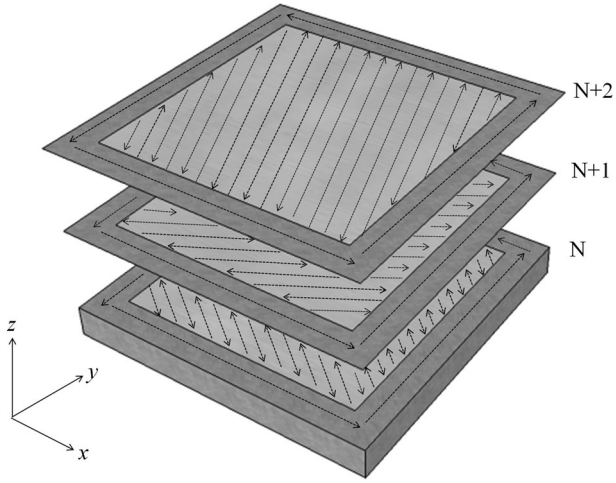

Fig. 1—Schematic diagram of the meander scan strategy: the laser scans the area of each layer with alternating parallel scan vectors. The border of each layer is then scanned twice. The scan rotation is rotated by 67 deg at each new layer deposition.

Ti-6Al-4V build plate pre-heated at 338.15 K (65.15 °C) in a protective Ar atmosphere.

The microstructure of the as-built components was studied from three orthogonal sections of the specimens, *i.e.*, the frontal, lateral, and horizontal planes (*xz*-, *yz*- and *xy*-planes according to ASTM F2921-11). Sample surfaces were prepared by standard metallographic preparation procedures and then etched in Kroll's solution for optical/SEM. The microstructure of the components was examined in a Reichert-Jung MEF3 optical microscope and a Carl Zeiss (Leo) 1530 VP field emission gun-SEM system. Energy dispersive X-ray spectroscopy (EDX) was used to identify the chemical composition of the powder, built components, and the existence of the secondary phases.

The distribution of crystallographic orientations of the sample crystals was studied using electron backscatter diffraction (EBSD) analysis on a FEI Nova 600 Nanolab Dualbeam FIB/FEG-SEM system with an EDAX EBSD camera. The crystallographic textures of the frontal and the lateral planes of the specimens (*xz*- and *yz*-planes, respectively) were studied on EBSD data sets acquired with a step size of 1 μm. Variant selection and orientation relationship of the martensitic α' grains were studied on EBSD data set from the three orthogonal planes (*i.e.*, frontal *xz*-, lateral *yz*-, and horizontal *xy*-planes) using an acquisition step size of 0.3 μm. EBSD data was processed using the TSL acquisition and data analysis software while the reconstruction of the β phase crystallographic texture was carried out using Matlab (The Mathworks, Inc., Natick, MA).

The reconstruction of high temperature β grains was based on the Burgers crystallographic relationship that governs the $\beta \rightarrow \alpha'$ phase transformation. It has, in fact, been reported that when at room temperature residual β phase is not present (as expected in as-built SLM components), the nucleation of β grains from the α laths during heating up into the β phase field follows the Burgers orientation relationship.[28,29] The orientations

of the parent β grains were computed considering every triplet of neighboring α' variants in the EBSD data set as suggested in References 21, 22. The α' orientation was initially expressed by a rotation matrix using the three Euler angles between the principal crystallographic axes for each α' grain and axes fixed by the geometry of the specimen (Appendix A). Using the Burgers orientation relationship, six possible parent phase (β grain) orientations were generated for every examined α' triplet. Only the solution common to the triplet (or the solution with the least misorientation) was taken as orientation of the parent β phase. Solutions exceeding a misorientation of 8 deg were discarded from the original dataset as a compromise to reconstruct the parent β phase with accuracy of 8 deg orientation spread. It also enabled the generation of an orientation map from a representative number of data points. Variant selection and variant frequency distribution were determined confronting the misorientation between the measured α' grain orientation and the 12 possible solutions generated by the corresponding parent β phase. The variant frequency distribution was calculated considering the α' grain that consisted at least of four collected points, thus α' grains equal or larger than ~1 μm.

III. RESULTS AND DISCUSSION

A. *General Microstructural Features of As-built SLM Components*

Ti-6Al-4V is an allotropic alloy that transforms fully into the β phase field above the β transus temperature [typically above 1223.15 K (950.15 °C)] and into a $\alpha + \beta$ phase mixture below this critical temperature. Nevertheless, the amount β phase retained at room temperature is governed by the cooling rate experienced from the β phase field.[30] During SLM, each layer cools down very rapidly (in the orders of thousands degrees per second)[31] and fully martensitic α' phase is expected to be present in the as-built Ti-6Al-4V components.

The optical microscopy analysis reveals that the microstructure of the components is composed of fine acicular α' grains throughout the sample and only prior β grain boundaries are left behind after the solidification (Figures 2(a) through (c)).[6–9] The frontal plane (xz-plane) shows continuous vertical prior β grain boundaries parallel to the build direction (Figure 2(a)). The presence of prior β columnar grain boundaries is due to the fact that Ti-6Al-4V solidifies in the β phase field and heat is mainly conducted away vertically.[31] Prior β grains have a lenticular morphology with an high aspect-ratio. The mid-length average width of the prior β grains is 103 ± 32 μm that corresponds to the chosen hatch spacing (100 μm). Prior β grains have a length in the order of millimeters. It is not clear to show in the micrograph where each layer deposition has occurred, however it can be estimated that β grains have grown through tens of layers as each powder bed layer on the scan platform was approximately 50 μm. Prior β columnar grain boundaries also emerge from the optical microscopy analysis of the lateral yz-plane (Figure 2(b)). Figure 2(b) shows that the prior β grain growth direction $\vec{g}$ is inclined ~20 deg to the build direction (z-axis) as a result of the adopted rotating scan strategy.[9] Although the scan vectors are hatching each layer in alternating

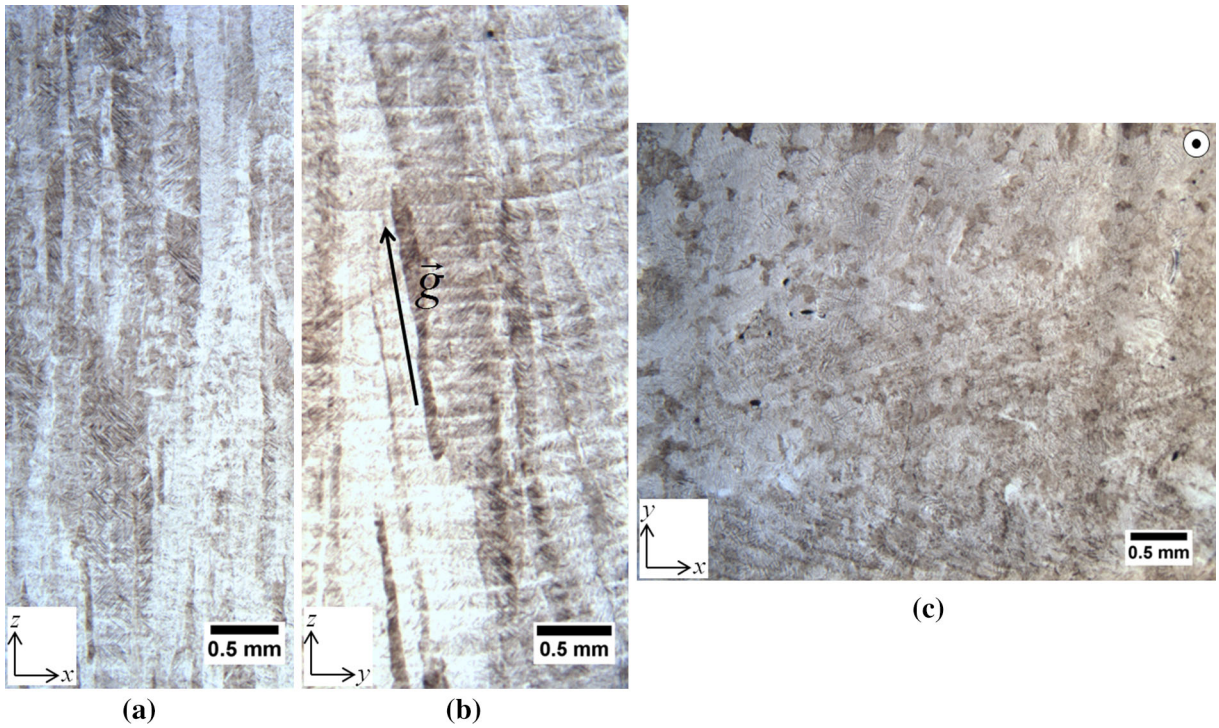

Fig. 2—(*a*) Optical micrograph from the frontal xz-plane, (*b*) lateral yz-plane, and (*c*) horizontal xy-plane of an as-deposited cubic component. Prior β columnar grain boundaries and α' lath appear in the microstructure. The vector $\vec{g}$ shows the β grain growth direction.

direction (Figure 1), it is reasonable to assume that the 67 deg rotation of the scan direction imposed by the scan strategy causes local heat gradients in the y direction (Figure 1). These thermal gradients would explain the inclination of the β grains shown in Figure 2(b). The horizontal plane (xy-plane) reveals the cross sections of the prior columnar β grains (Figure 2(c)) but the correlation between the scan strategy and the morphology of the prior β grains does not appear as clear as reported in other studies[9] probably due to the complexity of the meander scan strategy. Further heat transfer modeling is required to work out the detailed thermal gradient for this particular scan strategy.

As shown in Figures 2(a) through (c), α' grains do not vary in size along the build and scanning directions because the build platform was kept at a temperature much lower than the $\alpha + \beta$ annealing temperature for Ti-6Al-4V.[30] The build platform that acts as a heat sink did not affect the as-deposited α' phase size, different from that reported for EBM and laser metal deposited Ti-6Al-4V where the thermal mass offered by the components built on heated build platform has shown an important effect in the decomposition of non-equilibrium phases and the grain growth.[14,15]

The α' martensitic laths are organized within prior β grain boundaries with different inclinations mainly at

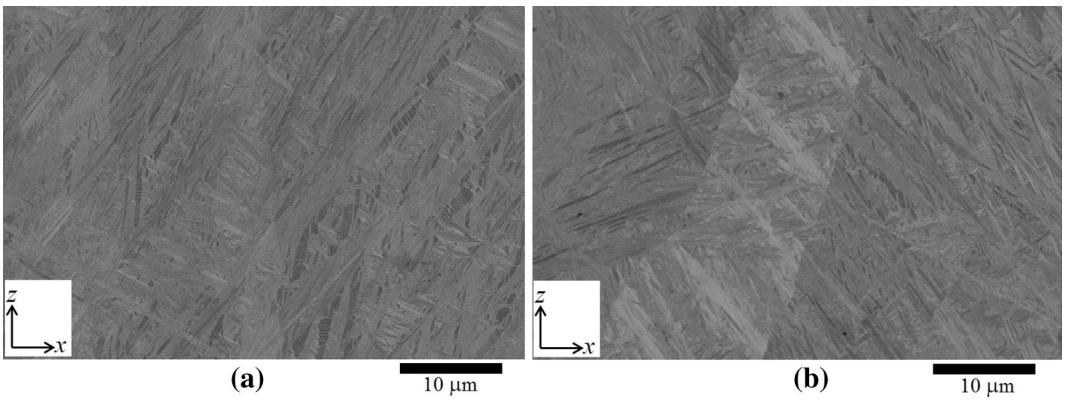

Fig. 3—(*a*) and (*b*) Backscattered electron micrographs showing the morphology and the arrangement of the α' laths within the prior β columnar grains.

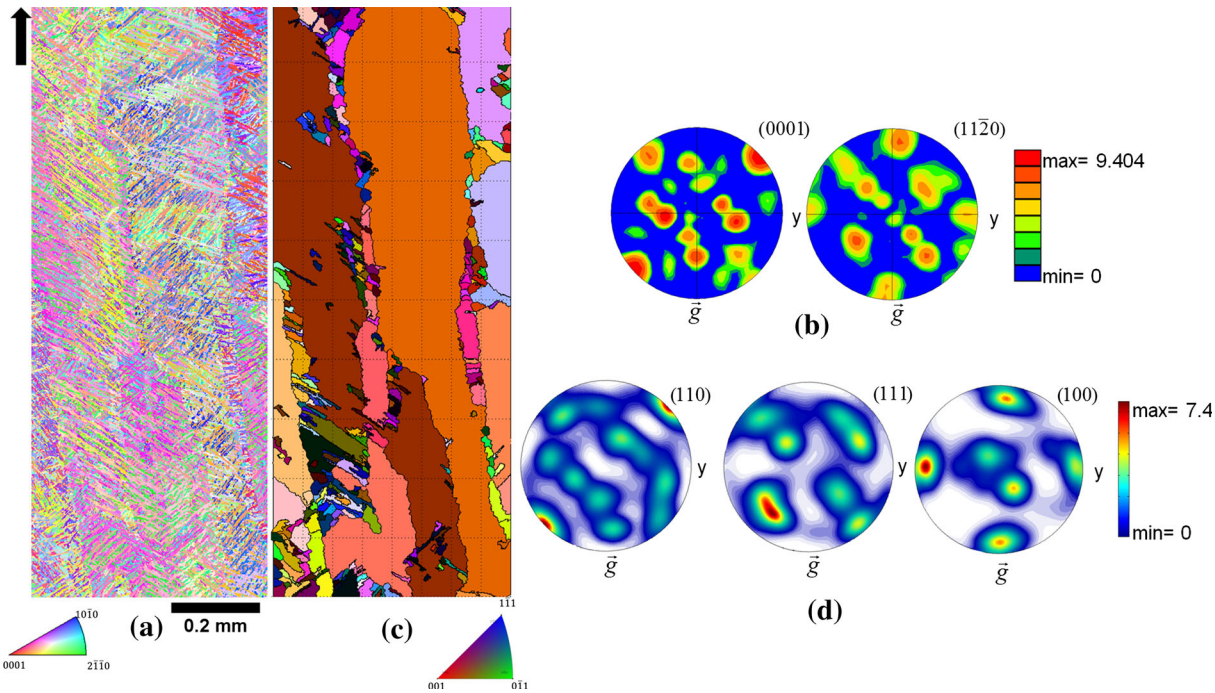

Fig. 4—(*a*) EBSD α' orientation map and the corresponding color scheme of a specimen taken from the lateral yz-plane of an as-deposited component (the black arrow indicates the building direction); (*b*) corresponding $(0001)_{\alpha'}$ and $(11\bar{2}0)_{\alpha'}$ contour pole figures; (*c*) orientation map of the reconstructed β phase. The black grain boundaries represent β grains misoriented equal or larger than 7 deg; (*d*) the corresponding (110), (111), (100) contour pole figures.

~±45 deg and ~90 deg to the build direction as shown in Figures 3(a) and (b).[7,8] The α′ grains do not precipitate along the β grain boundaries (Figure 3(b)) and this suggests that the α′ grains originate simultaneously from different points within the parent β grain which is typical of martensitic transformations. This microstructural morphology will be discussed in connection with the crystallographic texture of the α′ grains in Section III–B. The martensitic nature of the α′ grains was confirmed by studying the crystallographic structure and chemistry of the laths using TEM.[25] The α′ phase appeared as relatively long and narrow laths characterized by high vanadium content and high dislocation density.

B. *Texture Evolution of SLM Ti-6Al-4V*

In recent years crystallographic texture has been shown to be extremely useful to understand the relationship between processing and microstructure of a number of α/β Ti alloys to achieve desirable mechanical properties.[32,33]

In order to investigate the texture evolution occurring during SLM, specimens from the lateral *yz*-, frontal *xz*- and horizontal *xy*-planes of the as-deposited material were studied by EBSD. Figure 4(a) shows the α′ orientation map of the lateral plane (*yz*-plane) of the as-built cubic samples. No packets of α′ laths sharing the same crystallographic orientation (also known as α′ colonies) appear in the orientation map contrary to that reported for Ti-6Al-4V processed by shaped metal deposition and electron beam melting[15,34] probably because of the higher cooling rate experienced by the solidifying powder bed during SLM. The overall α′ texture appears random because of the relatively high number of α′ variants within each prior β grain (Figure 4(b)).

Figure 4(c) shows the corresponding reconstructed β orientation map whereas the contour pole figures of the α′ and the β phase are illustrated in Figures 4(b) and (d), respectively. The orientation map of the reconstructed β phase reveals that each β grain grows epitaxially extending through several deposited layers. The analysis of the corresponding contour pole figures shows a

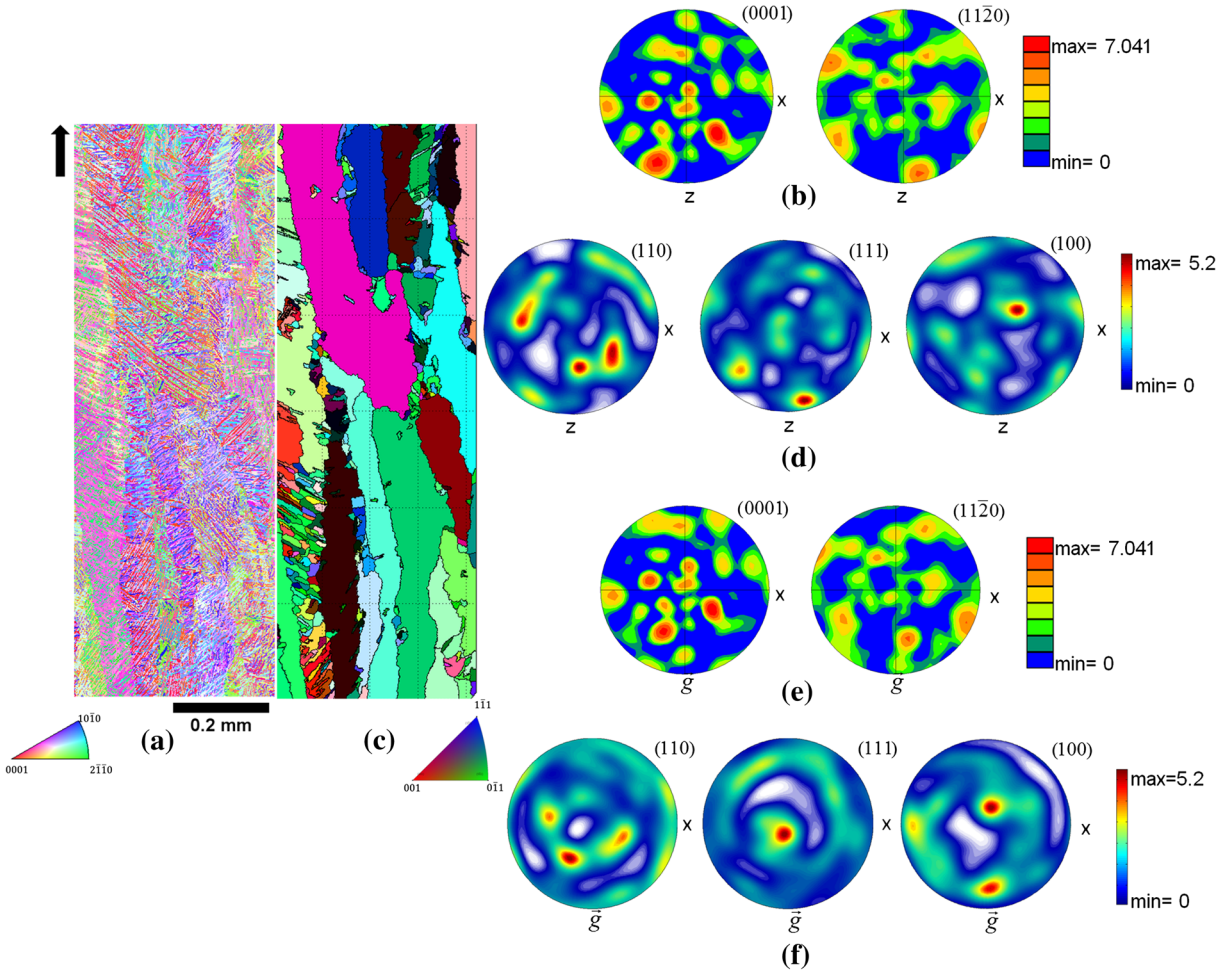

Fig. 5—(*a*) EBSD α′ orientation map and the corresponding color scheme of a specimen taken from the frontal *xz*-plane of an as-deposited component (the black arrow indicates the building direction); (*b*) corresponding $(0001)_{\alpha'}$ and $(11\bar{2}0)_{\alpha'}$ contour pole figures; (*c*) orientation map of the reconstructed β phase. The black grain boundaries represent β grains misoriented equal or larger than 7 deg; (*d*) the corresponding (110), (111), (100) contour pole figures; (*e*) $(0001)_{\alpha'}$ and $(11\bar{2}0)_{\alpha'}$ contour pole figures of the α′ data set following a rotation of ~20 deg around the *y*-axis; (*f*) (110), (111), (100) contour pole figures of the corresponding rotated β phase.

dominant {100} texture component in the direction of grain growth $\vec{g}$ that tends to develop because of the preferential {100} growth direction of cubic crystals during solidification.

The α' texture of the frontal plane (*xz*-plane) is shown in Figure 5(a). Similar to the lateral *yz*-plane, no α' colonies are present in the microstructure and the α' texture is weak (Figure 5(b)). The reconstruction of the corresponding high temperature β phase is shown in Figure 5(c). Although the orientation components shown in the pole figures (Figures 5(b) and (d)) not appear as {100} texture, by applying a rotation of ~20 deg around the *y*-axis (hence aligning the *z* direction with the inclined grain growth direction $\vec{g}$) produces the {100} texture components observed on the lateral plane (*yz*-plane) confirming that the {100} β grain growth direction is inclined ~20 deg to the build direction (Figures 5(e) and (f)).

High-resolution EBSD (0.3 μm acquisition step size) from two orthogonal planes (horizontal *xy*-plane Figure 6 and frontal *xz*-plane Figure 7) was also carried out to study in detail the orientation relationship among the α' variants, which formed within the columnar β grains and their relationship with the parent β phase.

As shown in Figures 6(b), (c), 7(b), and (c), typically, there are 5 to 6 variants that formed inside every parent β grain. The $(0001)_{\alpha'}$ plane of each α' lath is parallel to one of the $(110)_{\beta}$ planes of the reconstructed parent phase and at least one of the $\langle 11\bar{2}0\rangle_{\alpha'}$ directions is parallel to one of the $\langle 111\rangle_{\beta}$ proving that the reconstruction of the β phase was correct.

As indicated in Figures 6 and 7, clusters of three α' variants misoriented 63.26 deg apart around the $\langle \bar{1}0553\rangle_{\alpha'}$ axis (type 4[35]) or 60 deg around $\langle 11\bar{2}0\rangle_{\alpha'}$ (type 2[35]) are predominantly formed, whereas the remaining α' laths tend generally to form smaller clusters misoriented 60.83 deg misoriented around the $\langle \overline{1.3771}2.3770.359\rangle_{\alpha'}$ axis (type 3[35]). In the example of Figure 6(b) two α' variants are misoriented type 3 (marked by solid circles) whereas Figure 6(c) shows clusters of two α' variants misoriented type 4. Figure 7(b) shows the prior β grain has transformed into a cluster of three α' laths misoriented type 4 (marked by dotted oval) and a cluster of two α' laths misoriented type 3 (marked by solid circles). The β grain illustrated in Figure 7(c) is instead made of a cluster of three variants misoriented type 2 (marked by dashed ovals) and two remaining individual laths again misoriented type 3. From the analysis of the data sets, it is therefore reasonable to believe that the α' grains precipitate in order to satisfy the self-accommodation of the neighboring α grains[35] according to which small group α' variants would prefer to adopt two of the five types of possible grain boundary misorientation angles (*i.e.*, type

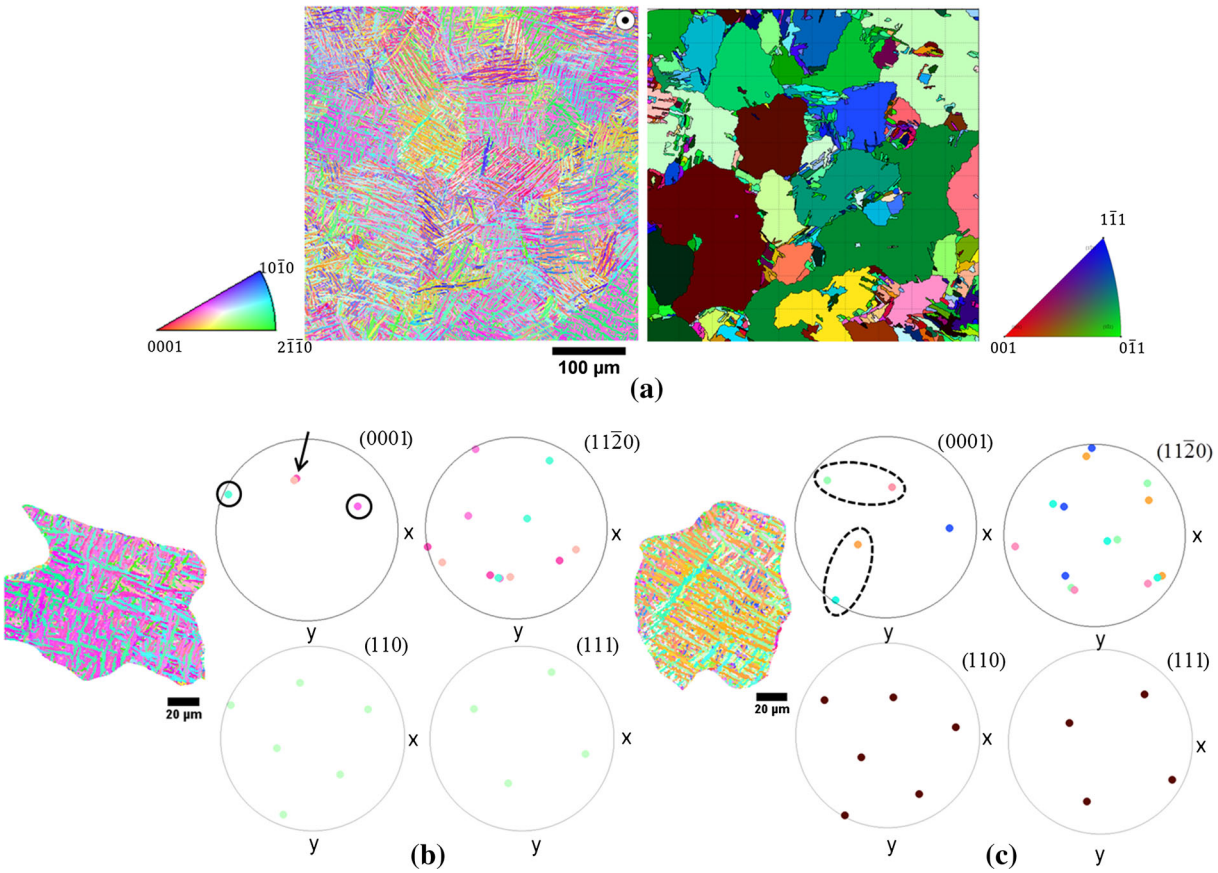

Fig. 6—(*a*) α' and corresponding reconstructed β orientation maps from the horizontal *xy*-plane (step size 0.3 μm); (*b*) and (*c*) discrete pole figures of the α' variants and their parent β grain. The arrow indicates α' laths that are misoriented type 6. The circles indicate α' laths that are misoriented type 3 whereas the dashed ovals show clusters of α' variants misoriented type 2.

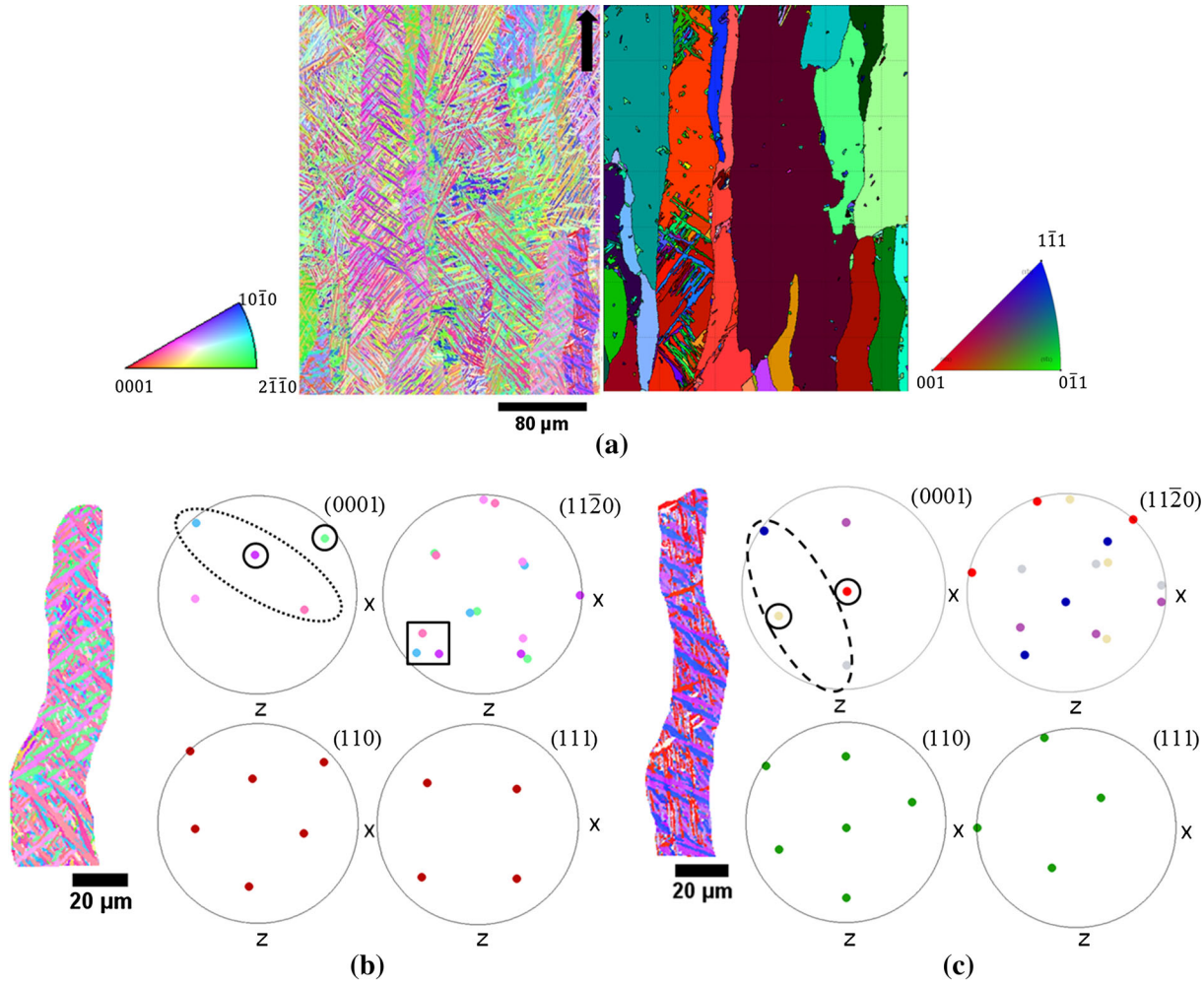

Fig. 7—(*a*) α′ and corresponding reconstructed β orientation maps from the frontal *xz*-plane (step size 0.3 μm). The black arrow shows the build direction; (*b*) and (*c*) discrete pole figures of the α′ variants and their parent β grain. The dotted ovals show clusters of α′ variants misoriented type 4 whereas the dashed ovals indicate α′ variants misoriented type 2. The circles indicate α′ laths that are misoriented type 3. α′ laths forming triangular patters are marked by a square.

2 and type 4) in order to minimize the average shape strain induced by the $\beta \rightarrow \alpha'$ transformation. Occasionally α′ grains share a $(0001)_{\alpha'}$ pole and have the three $(11\bar{2}0)_{\alpha'}$ reflections misoriented by 10.53 deg around the $\langle 0001 \rangle_{\alpha'}$ axes (type 6[35]) as indicated by the arrow in Figure 6. This particular orientation relationship derives from the sixfold symmetry of the α′ lattice and by the fact that during the $\beta \rightarrow \alpha'$ transformation the $\langle 11\bar{2}0 \rangle_{\alpha'}$ direction remains parallel to the two possible $\langle 111 \rangle_{\beta}$ close packed directions that lie on the $\{110\}_{\beta}$ plane.[36,37]

Triangular geometric patterns occur occasionally the $(11\bar{2}0)_{\alpha'}$ pole figures as shown in Figure 7(b) (marked by a square). These patterns occur when the basal reflections of different α′ grains are not parallel but one or two $(11\bar{2}0)_{\alpha'}$ reflections are shared, and therefore clusters of three variants misoriented type 4 are formed within the same β grain.

In addition, a careful analysis of Figure 7 reveals that even though β grains have grown through successive layer depositions, α′ laths with similar orientations have formed dominantly throughout the entire prior β grain. It is evident that during SLM, the α′ phase around the melt pool is heated into the β phase field and then rapidly cooled down to form the same α′ variants suggesting that texture inheritance/preferred variant selection might have taken place.[28,29] SLM involves remelting of the top portion of the deposited part together with a newly deposited layer of powders, thus as continuous $\alpha' \rightarrow \beta \rightarrow \alpha'$ transformations occur, a large number of α′ variant would form if texture inheritance/variant selection did not take place.

As shown in the example of Figure 8, three dominant α′ orientations are observed due to the preferred variant selection within the same prior β grain as indicated in the $(0001)_{\alpha'}$ and $(11\bar{2}0)_{\alpha'}$ pole figures of the corresponding grains. More specifically, it was observed that the α′ laths indicated with the same color in Figure 8(a) represent the same variant and were misoriented less than 5 deg despite having formed during successive layer depositions.

Although texture inheritance has never been reported for Ti-6Al-4V made by AM technologies, as shown in this study, the β grains grow epitaxially and maintain a strong {100} texture during the $\alpha' \rightarrow \beta$ phase transformation associated with the re-melting of successive

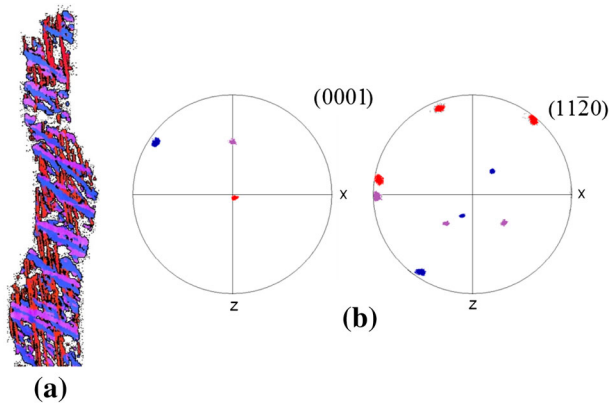

Fig. 8—(*a*) Detail from the frontal *xz*-plane orientation map showing that the prior β columnar grain is composed of three α' variants that repeat during successive depositions; (*b*) corresponding $(0001)_{\alpha'}$ and $(11\bar{2}0)_{\alpha'}$ discrete pole figures.

layers. As a result, just one preferred variant among the six possible solutions for the $\alpha' \rightarrow \beta$ transformation seems to have occurred.

During the cooling of the layers (*i.e.*, the $\beta \rightarrow \alpha'$ transformation) variant selection at special prior β grain boundaries has been suggested.[36,37] Thus the orientation relationship of the α' grains across prior β grain boundaries was also investigated. Figure 9(a) shows two prior β grains A and B which are 8 deg misoriented and therefore meet the criteria for variant selection at the grain boundary.[38] It was observed that the α' laths formed in the corresponding β grains shown no orientation relationship and thus preferred variant selection across the boundary. In particular, the example of Figure 9(b) shows that one $(110)_{\beta}$ and one $(111)_{\beta}$ plane in those two β grains are almost parallel (indicated by the arrows in Figure 9(b)) but the α' variants that have formed in each β grain, have none of the $(0001)_{\alpha'}$ planes that has remained parallel to that shared $(110)_{\beta}$.

Studying other examples in the same dataset, it was also observed that the reconstructed β grains have in general high angle grain boundaries misorientation. This suggests that selection of α' variants of same orientation on both sides of the neighboring β grains might thus not be beneficial to lower the α' nucleation energy during the $\beta \rightarrow \alpha'$ transformation as reported in References 36 through 38. In turn, variant selection at prior β grain boundaries seems unlikely during SLM of Ti-6Al-4V.

It was observed however that α' variants of similar inclination to the growth direction have the same crystal orientation shown by the same color (Figure 8). This suggests that during the $\beta \rightarrow \alpha'$ transformation certain variants might have been chosen preferably to minimize the work associated with the stresses and strains involved in the phase transformation as reported.[39,40] Similar mechanisms of local variant selection might take place during SLM.

To verify whether certain α' variants occurred more frequently, statistics regarding the variant frequency was determined for the data sets acquired on two orthogonal planes (horizontal *xy*- and frontal *xz*-planes, respectively). It was observed that during the $\beta \rightarrow \alpha'$ all the 12

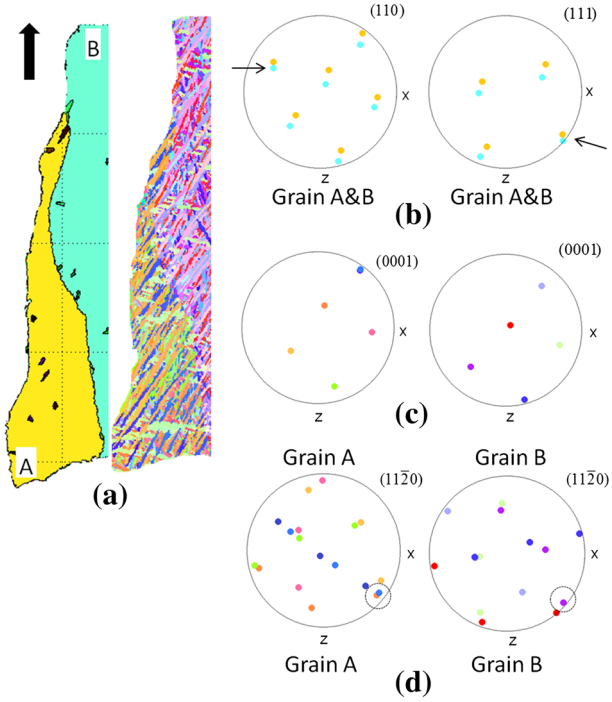

Fig. 9—(*a*) EBSD orientation map of two reconstructed adjacent β grains and their α' variants; (*b*) superimposition of the $(110)_{\beta}$ and $(111)_{\beta}$ pole figures of the prior β grains (orange and light-blue reflections corresponding to the prior β grains A and B respectively). The arrows indicate pole reflections that are almost parallel to each other; (*c*) $(0001)_{\alpha'}$ and (*d*) $(11\bar{2}0)_{\alpha'}$ pole figures of the α' variants deriving from the two grains (Color figure online).

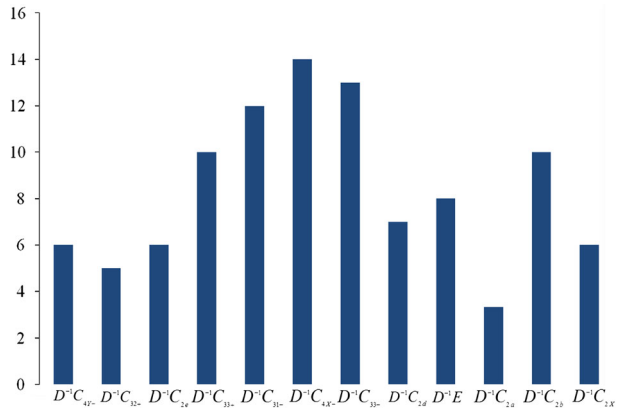

Fig. 10—Variant frequency distribution from the data sets analyzed in Figs. 6 and 7.

variants occurred but 6 of the 12 solutions constitute about 70 pct of the data sets (Figure 10). Among the six variants that occur more frequently, it was observed that variants that are misoriented type 6 (for example solutions $D^{-1}C_{31-}$ and $D^{-1}C_{4X-}$),[35] type 2 (*e.g.*, solutions $D^{-1}C_{33+}$ and $D^{-1}C_{4X-}$),[35] or type 4 (*e.g.*, solutions $D^{-1}C_{33+}$ and $D^{-1}E$),[35] dominate for all the three orthogonal planes consistently with that observed on the discrete pole figures of Figures 6 and 7.

It is noteworthy that the variant frequency distribution was determined for all the α' grains equal or larger

than about 1 μm. It is possible therefore that the small α' grains (~1 μm in size) had precipitated within the columnar β grain following no preferred variant selection, explaining the fact that all the 12 solutions are observed in Figure 10.

The present work has helped to understand the microstructure formation of Ti-6Al-4V processed by SLM with major focus on the texture evolution. The results presented enhance the ability to predict the final microstructure and its evolution from the choice of specific set of process parameters that enabled the production of near fully dense components.

IV. CONCLUSIONS

It has been shown that the as-fabricated components consist entirely of α' martensitic phase in prior columnar β. It was demonstrated that the prior β columnar grains are formed due to the epitaxial solidification across the deposited layers.

The crystallographic texture of the samples was studied on three orthogonal planes. It was found that prior β grains have a preferred {100} texture along the main grain growth direction which is inclined ~20 deg to the build direction (z-axis). The orientation relationship of the α' grains precipitated within the columnar grains and their parent β phase was examined. As predicted, it was proved that the $\beta \rightarrow \alpha'$ transformation is governed by the Burgers orientation relationship: most of the α' laths belonging to the same parent β grain have the $(0001)_{\alpha'}$ reflection 60 deg misoriented around the $\langle 01\bar{1}0 \rangle_{\alpha'}$ axes. The $(11\bar{2}0)_{\alpha'}$ pole figures reveal that the α' variants precipitate in clusters forming boundary misorientations that minimize the strain energy associated with martensitic transformation. During the deposition of successive layers texture inheritance seems to occur within prior β grains. α' grains of similar inclination have the same crystal orientation. Although variant selection at prior β grain boundaries is unlikely due to the fast cooling that occurs during SLM it is possible that certain variants might be chosen among others to minimize the phase transformation energy. The overall α' texture, however, appears random because of the large number of micron sized α' grains that precipitate within the columnar β grains grow in multiple directions and random orientation was evidenced by the variant frequency distribution.

It was found that the adopted rotating scan strategy has a strong influence on the solidification texture and, in consequence, on the development of the final microstructure. As a future work the solidification cooling rates and the thermal gradients deriving from the choice of different laser scan strategy will be investigated.

The fully martensitic microstructure suggests that SLM Ti-6Al-4V will exhibit high strength but low ductility. In addition, the lack of α colonies and the presence of elongated prior β grain boundaries in the microstructure indicate that the predominant mode of failure might be intergranular. For this reason, the orientation of prior β grain boundaries (*i.e.*, the build orientation) relative to the external loading could affect sensibly the mechanical performance of the parts. Further research on the detailed fracture mechanism in relation to the microstructure of the SLM Ti-6Al-4V parts is required.

APPENDIX A

One method to express the 3D orientation of a crystal is to define the rotation of the crystal coordinate system relative to the sample coordinate system and consider the symmetry of the crystal itself. The rotation of the crystal is generally described by a triplet of angles, known as Euler angles, (φ_1, Φ, φ_2), that express the consecutive rotations about the axis of the crystal coordinate system that are needed to bring the crystal coordinate system into coincidence with the sample coordinate system (*i.e.*, passive rotations). In the present study a crystal coordinate system for the α and β phases was chosen as defined in the software OIM TM 5.2 of the EDAX-TSL system. The 3D rotations were then expressed according to the Bunge's convention as follow:

$$R(\varphi 1, \varphi, \varphi 2) = \begin{bmatrix} \cos\varphi 1 \cos\varphi 2 - \sin\varphi 1 \sin\varphi 2 \cos\varphi & \sin\varphi 1 \cos\varphi 2 + \cos\varphi 1 \sin\varphi 2 \cos\varphi & \sin\varphi 2 \sin\varphi \\ -\cos\varphi 1 \sin\varphi 2 - \sin\varphi 1 \cos\varphi 2 \cos\varphi & -\sin\varphi 1 \sin\varphi 2 + \cos\varphi 1 \cos\varphi 2 \cos\varphi & \cos\varphi 2 \sin\varphi \\ \sin\varphi 1 \sin\varphi & -\cos\varphi 1 \sin\varphi & \cos\varphi \end{bmatrix}$$

Because of the crystal symmetry however, multiple rotations can result in an equivalent 3D orientation of a certain crystal. For this reason, it was also necessary to take into account the rotational symmetry elements of α and β phases in order to be able to distinguish independent orientations. The rotational symmetry elements of the α and β phases (12 and 24, respectively) used in this study are listed in the form of rotational matrices (Bunge's convention) in Tables I and II.[22] As the α and β phases are related through the Burgers orientation relationship which is equivalent to a Bunge's rotation expressed by the matrix D (135, 90, 325 deg), it has been shown that starting from three α grain orientations it is possible to the determine the parent β grain orientation with accuracy and conversely each β grain can generate 12 distinct α grain orientations (α variants).[21,22] In the present study, the 12 α variants generated from one single β grain correspond to the set of rotations listed in Table III.

Table I. Rotational Elements of the Cubic Symmetry

$E(0,0,0)$	$C_{4x+}(0,\pi/2,0)$
$C_{2x}(0,\pi,0)$	$C_{4y+}(\pi/2,\pi/2,3\pi/2)$
$C_{2y}(\pi,\pi,0)$	$C_{4z+}(\pi/2,0,0)$
$C_{2z}(\pi,0,0)$	$C_{4x-}(\pi,\pi/2,\pi)$
$C_{31+}(\pi/2,\pi/2,0)$	$C_{4y-}(3\pi/2,\pi/2,\pi/2)$
$C_{32+}(3\pi/2,\pi/2,\pi)$	$C_{4z-}(3\pi/2,0,0)$
$C_{33+}(3\pi/2,\pi/2,0)$	$C_{2a}(\pi/2,\pi,0)$
$C_{31-}(\pi,\pi/2,\pi/2)$	$C_{2b}(3\pi/2,\pi,0)$
$C_{32-}(0,\pi/2,3\pi/2)$	$C_{2c}(\pi/2,\pi/2,\pi/2)$
$C_{33-}(\pi,\pi/2,3\pi/2)$	$C_{2d}(\pi,\pi/2,0)$
$C_{34-}(0,\pi/2,\pi/2)$	$C_{2e}(3\pi/2,\pi/2,3\pi/2)$
$C_{34+}(\pi/2,\pi/2,\pi)$	$C_{2f}(0,\pi/2,\pi)$

Table II. Rotational Elements of the Hexagonal Symmetry

$E(0,0,0)$	${}^{H}C'_{21}(\pi,\pi,0)$
${}^{H}C_{6z+}(\pi/3,0,0)$	${}^{H}C''_{22}(\pi,\pi,\pi/3)$
${}^{H}C_{3z+}(2\pi/3,0,0)$	${}^{H}C'_{23}(\pi,\pi,2\pi/3)$
${}^{H}C_{2x}(0,0,\pi)$	${}^{H}C''_{21}(\pi,\pi,\pi)$
${}^{H}C_{3z-}(4\pi/3,0,0)$	${}^{H}C'_{22}(\pi,\pi,4\pi/3)$
${}^{H}C_{6z-}(-\pi/3,0,0)$	${}^{H}C''_{23}(\pi,\pi,5\pi/3)$

Table III. α Grain Rotations Deriving from a Single Parent β Grain

1. $D^{-1}C_{4Y-}$
2. $D^{-1}C_{32+}$
3. $D^{-1}C_{2e}$
4. $D^{-1}C_{33+}$
5. $D^{-1}C_{31-}$
6. $D^{-1}C_{4X-}$
7. $D^{-1}C_{33-}$
8. $D^{-1}C_{2d}$
9. $D^{-1}E$
10. $D^{-1}C_{2a}$
11. $D^{-1}C_{2b}$
12. $D^{-1}C_{2X}$

REFERENCES

1. M. Baumers, C. Tuck, R. Wildman, I. Ashcroft, and R. Hague: *Proceedings of the Solid Freeform Fabrication Symposium,* 2011.
2. C. Tuck, R. Hague, and N. Burns: *Int. J. Serv. Oper. Manag.*, 2007, vol. 3, pp. 1–22.
3. L. Murr, S. Quinones, S. Gaytan, M. Lopez, A. Rodela, E. Martinez, D. Hernandez, F. Medina, and R. Wicker: *J. Mech. Behav. Biomed.*, 2009, vol. 2, pp. 20–32.
4. A. Gebhardt, F. Schmidt, J. Hötter, W. Sokalla, and P. Sokalla: *Phys. Procedia*, 2010, vol. 5B, pp. 543–49.
5. E. Chlebus, B. Kuznicka, T. Kurzynowski, and B. Dybala: *Mater. Charact.*, 2011, vol. 62, pp. 488–95.
6. L. Facchini, E. Magalini, P. Robotti, A. Molinari, S. Hoeges, and K. Wissenbach: *Rapid Prototyp. J.*, 2010, vol. 16, pp. 450–59.
7. B. Vrancken, L. Thijs, J.P. Kruth, and J.V. Humbeeck: *J. Alloy. Compd.*, 2012, vol. 54, pp. 177–85.
8. T. Sercombe, N. Jones, R. Day, and A. Kop: *Rapid Prototyp. J.*, 2008, vol. 14, pp. 300–04.
9. L. Thijs, F. Verhaeghe, T. Craeghs, J.V. Humbeeck, and J.P. Kruth: *Acta Mater.*, 2010, vol. 58, pp. 3303–12.
10. D. Gu, Y. Hagedorn, W. Meiners, G. Meng, R.J.S. Batista, K. Wissenbach, and R. Poprawe: *Acta Mater.*, 2012, vol. 60, pp. 3849–60.
11. T. Vilaro, C. Colin, and J.D. Bartout: *Metall. Mater. Trans. A*, 2011, vol. 42A, pp. 3190–99.
12. B. Song, S. Dong, B. Zhang, H. Liao, and C. Coddet: *Mater. Des.*, 2012, vol. 35, pp. 120–25.
13. B. Baufeld and O.V. Biest: *Sci. Technol. Adv. Mater.*, 2009, vol. 10, p. 015008.
14. B. Baufeld, E. Brandl, and O.V. Biest: *J. Mater. Process. Technol.*, 2011, vol. 211, pp. 1146–58.
15. S. Al-Bermani, M. Blackmore, W. Zhang, and I. Todd: *Metall. Mater. Trans. A*, 2010, vol. 41A, pp. 3422–34.
16. S. Kelly and S. Kampe: *Metall. Mater. Trans. A*, 2004, vol. 35A, pp. 1861–67.
17. L. Zhang, D. Klemm, J. Eckert, Y. Hao, and T. Sercombe: *Scripta Mater.*, 2011, vol. 65, pp. 21–24.
18. T. Vilaro, V. Kottman-Rexerodt, M. Thomas, C. Colin, P. Bertrand, L. Thivillon, S. Abed, V. Ji, P. Aubry, P. Peyre, and T. Malot: *Adv. Mater. Res.*, 2010, vols. 89–91, pp. 586–91.
19. G.C. Obasi, S. Birosca, D.G. Leo, J. Prakash, Quinta da Fonseca, and M. Preuss: *Acta Mater.*, 2012, vol. 60, pp. 6013–24.
20. G.C. Obasi, S. Birosca, J. Quinta da Fonseca, and M. Preuss: *Acta Mater.*, 2012, vol. 60, pp. 1048–58.
21. M. Humbert, F. Wagner, H. Moustahfid, and C. Esling: *J. Appl. Crystallogr.*, 1995, vol. 28, pp. 571–76.
22. M. Humbert, N. Gey, J. Muller, and C. Esling: *J. Appl. Crystallogr.*, 1996, vol. 29, pp. 662–66.
23. M.G. Glavicic, P.A. Kobryn, T.R. Bieler, and S.L. Semiatin: *Mater. Sci. Eng. A*, 2003, vol. 351, pp. 258–64.
24. M.G. Glavicic, P.A. Kobryn, T.R. Bieler, and S.L. Semiatin: *Mater. Sci. Eng. A*, 2003, vol. 346, pp. 50–59.
25. M. Simonelli, C. Tuck, and Y.Y. Tse: *J Phys Conf Ser*, 2012, vol. 371 (1), p. 012084.
26. Renishaw Apply Innovation, 2012. http://www.renishaw.com/en/am250-laser-melting-machine–15253. Accessed Feb 2014.
27. M. Simonelli, Y.Y. Tse, and C. Tuck: *Proceedings of the Solid Freeform Fabrication Symposium,* 2012.
28. I. Lonardelli, N. Gey, H. Wenk, M. Humbert, S.C. Vogel, and L. Lutterotti: *Acta Mater.*, 2007, vol. 55, pp. 5718–27.
29. M.R. Daymond, R.A. Holt, S. Cai, P. Mosbrucker, and S.C. Vogel: *Acta Mater.*, 2010, vol. 58, pp. 4053–66.
30. R. Boyer and E.W. Collings: *Materials Properties Handbook: Titanium Alloys*, ASM International, Materials Park, OH, 1994, pp. 483–633.
31. I.A. Roberts, C.J. Wang, R. Esterlein, M. Stanford, and D.J. Mynors: *Int. J. Mach. Tool Manuf.*, 2009, vol. 49, pp. 916–23.
32. M.G. Glavicic, P. Kobryn, and S.L. Semiatin: *Mater. Sci. Eng. A*, 2004, vol. 385, pp. 372–76.
33. P. Kobryn and S.L. Semiatin: *J. Mater. Process. Technol.*, 2003, vol. 135, pp. 330–39.
34. B. Baufeld, O.V. Biest, and S. Dillien: *Metall. Mater. Trans. A*, 2010, vol. 41A, pp. 1917–27.
35. S.C. Wang, M. Aindow, and M.J. Starink: *Acta Mater.*, 2003, vol. 51, pp. 2485–2503.
36. D. Bhattacharyya, G. Viswanathan, R. Denkenberger, D. Furrer, and H.L. Fraser: *Acta Mater.*, 2003, vol. 51, pp. 4679–91.
37. D. Bhattacharyya, G.B. Viswanathan, and H.L. Fraser: *Acta Mater.*, 2007, vol. 55, pp. 6765–78.
38. N. Stanford and P.S. Bate: *Acta Mater.*, 2004, vol. 52, pp. 5215–24.
39. M. Humbert, L. Germaine, N. Gey, P. Bocher, and M. Jahazi: *Mater. Sci. Eng. A*, 2006, vol. 430, pp. 157–64.
40. G.A. Sargent, K.T. Kinsel, A.L. Pilchak, A.A. Salem, and S.L. Semiatin: *Metall. Mater. Trans. A*, 2012, vol. 43A, pp. 3570–85.